X68-134249

DECLASSIFIED

UB
NASA TM X-1493

NASA TECHNICAL MEMORANDUM

UB
NASA TM X-1493

FORWARD PENETRATION OF LIQUID WATER AND LIQUID NITROGEN INJECTED FROM AN ORIFICE AT THE STAGNATION POINT OF A HEMISPHERICALLY BLUNTED BODY IN HYPERSONIC FLOW

by Dennis M. Bushnell and Jarrett K. Huffman

Langley Research Center

Langley Station, Hampton, Va.

NATIONAL AERONAUTICS AND SPACE ADMINISTRATION • WASHINGTON, D. C. • MARCH 1968

FORWARD PENETRATION OF LIQUID WATER AND LIQUID NITROGEN

INJECTED FROM AN ORIFICE AT THE STAGNATION POINT OF

A HEMISPHERICALLY BLUNTED BODY

IN HYPERSONIC FLOW

By Dennis M. Bushnell and Jarrett K. Huffman

Langley Research Center
Langley Station, Hampton, Va.

NATIONAL AERONAUTICS AND SPACE ADMINISTRATION

FORWARD PENETRATION OF LIQUID WATER AND LIQUID NITROGEN

INJECTED FROM AN ORIFICE AT THE STAGNATION POINT OF

A HEMISPHERICALLY BLUNTED BODY

IN HYPERSONIC FLOW*

By Dennis M. Bushnell and Jarrett K. Huffman
Langley Research Center

SUMMARY

Measurements have been made of the maximum forward penetration of liquid water injected from the stagnation region of a hemisphere-cylinder at Mach numbers of 8 and 19.5. On the basis of a flow-field analysis, these data were correlated in terms of the liquid density and initial liquid velocity, free-stream density and velocity, vapor pressure and surface tension of the liquid, and free-stream Reynolds number based on nose diameter. It was found that the forward penetration was not a function of the injection-orifice diameter.

Measurements were also made with liquid nitrogen as the injectant at a Mach number of 8, and it was found that the penetration did not correlate with the same parameters as for the water injection tests because of the much greater evaporation rates of the liquid nitrogen. Since only limited data were obtained for cases involving evaporation, correlation parameters applicable to such cases could not be obtained except for the situation where evaporation was appreciable and therefore was probably the dominant mechanism affecting penetration.

INTRODUCTION

Stagnation-point liquid injection is currently of interest with regard to alleviation of the radio attenuation which occurs during atmospheric entry of spacecraft. As discussed in reference 1, the injection of water from the stagnation region during the RAM B2 flight resulted in appreciable signal recovery.

A further application for stagnation-point water injection was considered in reference 2, where preliminary results were reported which indicated that large cooling effects could be obtained for flat-faced bodies, hemisphere-cylinders, and 40° half-angle cones. The water flow rates and subsequent cooling effects were similar for all three

---

*Title, Unclassified.

configurations. These effects of stagnation-point water injection presumably depend in part on the distance the injected liquid penetrates ahead of the vehicle nose.

Investigations have been made of the penetration obtained with cross-stream liquid injection into subsonic flows (ref. 3) and supersonic flows (ref. 4). A limited amount of data for contrastream (stagnation region) liquid injection into supersonic flows is contained in reference 5.

The purpose of the present investigation was to determine the extent to which the bow shock of a blunt configuration in hypersonic flow would be modified by liquid injection from a single orifice at the stagnation point and to determine an empirical expression for the maximum penetration obtained. Tests were carried out with a hemisphere-cylinder at Mach numbers of 8 and 19.5, and the following quantities were varied: free-stream density and velocity; liquid density and velocity; vapor pressure, surface tension, and heat of vaporization of the liquid; and injection-orifice diameter.

Existing unpublished data for stagnation-point water injection at Mach numbers of 6 and 17.5 with a hemispherically blunted 9^0 cone are described in an appendix. During these tests the model nose diameter, injection-orifice diameter, free-stream density and velocity, liquid velocity, and vapor pressure were varied. The results are used to corroborate the final correlation of the present investigation.

SYMBOLS

A defined by equation (A12)

a,b distances (defined in fig. 8)

C_1,C_2 constants of integration

C_D drag coefficient

c_p specific heat

D model nose diameter

d_o orifice diameter

F_D drag force

f fraction of initial free-stream stagnation enthalpy present in separated flow region

H_{f_g} heat of vaporization of liquid

h   flow-field thickness at shoulder (fig. 8)

K   ratio of the flow rate of evaporated liquid to that of incoming air in stream tube of diameter D (expression (8))

k   thermal conductivity

L   initial radius characteristic of idealized liquid drop

l length of orifice (fig. 1)

M   Mach number

$\dot{m}_l$ flow rate of liquid from orifice

N_{Nu} Nusselt number

N_{Re} free-stream Reynolds number based on nose diameter

N_{We} maximum effective critical Weber number, Lp_v/σ

n   exponent

p   pressure

p_v vapor pressure of liquid

$R = r/L$

$\bar{R}$ gas constant

r   local particle radius

$\bar{r}$ radius of incoming airstream (fig. 8)

T   temperature

t   time

V	velocity
x	coordinate in negative wind direction
α	flow turning angle for shock having angle θ
δ	maximum penetration of liquid, measured from surface of model
θ	conical shock angle (fig. 8)
μ	viscosity
ρ	density
σ	surface tension of liquid
ψ	cone half-angle corresponding to conical shock angle θ

Subscripts:

av	mean effective flow-field condition at model shoulder
d	drop
g	gas
l	liquid conditions at exit of injection orifice
t	free-stream stagnation condition
tot	total value
V	vapor at $T = T_{w,d}$
w	wall
∞	free stream

1   portion covered by separated flow region.

2   portion over which attached flow occurs

APPARATUS

Tunnels

The Mach 8 tests were conducted in the Langley Mach 8 variable-density tunnel. This tunnel is of the blowdown type and has an axially symmetric nozzle with contoured walls. The average variation of test-section Mach number with stagnation pressure is given in reference 6. The test gas is dry air. For the present tests the stagnation pressure was varied from 200 to 900 psia (1.38 to 6.2×10^6 N/m^2). The corresponding free-stream Mach number range was 7.8 to 7.95. For the present tests the stagnation temperature varied from 840° F to 1000° F (722° K to 811° K).

The Mach 19.5 tests were conducted in the Langley hypersonic nitrogen facility. This tunnel is also of the blowdown type with an axially symmetric contoured nozzle. The facility has recently been put into operation and preliminary calibrations indicate that the nominal free-stream Mach number is 19.5 over the stagnation-pressure range of the present tests, which was from 4500 to 6700 psia (3.1 to 4.61×10^7 N/m^2). The nominal stagnation temperature was 2300° F (1534° K).

Model and Instrumentation

The model used in the present investigation was a hemispherically blunted cylinder 0.1198 ft (0.036 m) in diameter. The model was constructed of type 347 stainless steel and was provided with a receptacle drilled in the nose for installation of injection nozzles. A sketch of the model and injection nozzles is given in figure 1. A 30 gage (0.010 in., 0.025 cm) swaged-wire copper-constantan thermocouple and a pressure orifice with 0.040 in. (0.10 cm) inside diameter were located as shown to monitor the temperature and pressure of the liquid in the entrance passage. The exit passage was used as a bypass line to precool the model for the liquid-nitrogen injection tests. Each of the three nozzles used for the present tests had a single orifice. The orifice diameters, l/d_o ratios, and entrance angle are given in figure 1.

The liquid supply system consisted of a bottle connected to the model and pressurized to the desired level with gaseous nitrogen.
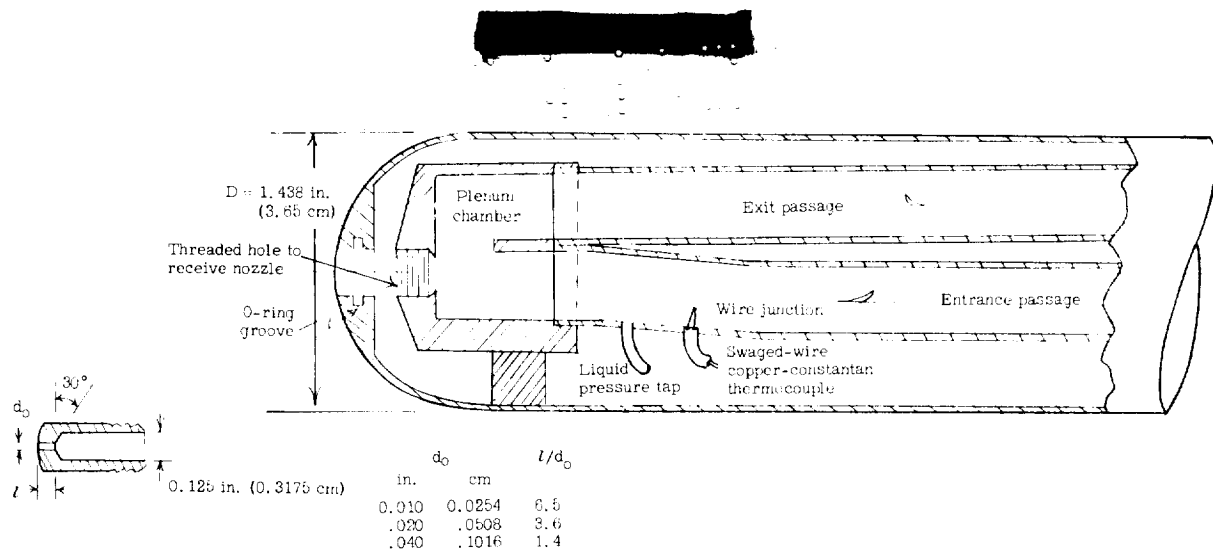
Figure 1.- Sketch of model and injection nozzles.

TEST PROCEDURES AND DATA REDUCTION

Liquid-Nitrogen Injection

For the liquid-nitrogen tests the model and associated piping were first cooled to liquid-nitrogen temperatures at a low coolant flow rate with the model in the test position but the tunnel not in operation. The liquid injection system was then rapidly pressurized to the desired injection pressure, and the tunnel was started. The injectant temperature and pressure were monitored, and when these values became steady, several spark schlieren photographs were taken. In general, the photographs showed different amounts of penetration, as the flow field was found to be unsteady, but the photograph which showed the maximum penetration was used for data-reduction purposes. Whether the penetration measured was actually the maximum is discussed subsequently. The most forward position of the model bow shock was assumed to represent the maximum penetration. The initial liquid velocity was obtained from the incompressible form of the Bernoulli equation as written between the liquid-pressure measuring station and the nozzle exit. To insure the validity of this approach, the total pressure in the model plenum chamber was always kept larger than the local vapor pressure so that single-phase conditions existed in the entrance to the nozzle. The liquid-nitrogen injection tests were conducted only at a Mach number of 8, at angles of attack from 0° to 6°.

Water Injection

The test procedure for the water-injection tests was similar to that for the liquid-nitrogen tests except that precooling was unnecessary. An oil-bath heat exchanger was used to obtain injection water temperatures higher than ambient. The water-injection tests were carried out at Mach numbers of 8 and 19.5. The free-stream properties for

6

the tests at a Mach number of 19.5 were obtained by applying correction factors given in reference 7 to the ideal gas values. All tests were conducted with the model at zero angle of attack. As in the liquid-nitrogen tests, the initial liquid velocity was obtained from the incompressible form of the Bernoulli equation as written between the liquid-pressure measuring station and the nozzle exit. This procedure is justified by pitot surveys of the exit region of similar nozzles, which indicated negligible losses between the plenum chamber and the exit.

ACCURACY

The major source of error in the present tests is the fact that only a few schlieren photographs (less than 10) were taken during a given test. Therefore, as the flow field was unsteady, the maximum extent of the penetration may not have been photographed. This error would lead to lower than actual values of maximum penetration. The amount of uncertainty involved is probably on the order of 30 percent of the observed value, based on the magnitude of the flow-field oscillations. Also, if the liquid temperatures at the measuring station and the exit of the orifice were different as a result of heat transfer between liquid and model, the value of the vapor pressure could be decidedly different because of the large dependence of vapor pressure upon temperature. These errors in vapor pressure are probably of the order of 20 percent.

RESULTS AND DISCUSSION

Flow Field

Shown in figure 2 are typical schlieren photographs for liquid-nitrogen and water injection at a Mach number of 8. As mentioned previously, the flow field was observed to be unsteady during injection. The type of flow-field oscillations encountered in the liquid-nitrogen tests can be seen in figures 2(a) and 2(b), which are for the same test conditions. (The white areas in these photographs are extraneous reflections from a light beam used to study liquid-droplet distribution.) Figure 2(a), which depicts maximum penetration, shows a pointed conical shock which extends far out in front of the normal bow-shock location. In figure 2(b), which depicts minimum penetration, the shock is no longer pointed and the flow field is broken up into a series of bow waves. These shock shapes are typical of those observed with maximum and minimum penetration in the liquid-nitrogen injection tests. There did not appear to be any difference in penetration between the 0° and 6° angles of attack.

An example of maximum penetration for water injection is shown in figure 2(c). Again the shock is pointed. However, during the water-injection tests the general shock shape remained pointed even for minimum penetration. Also, a discrete liquid jet
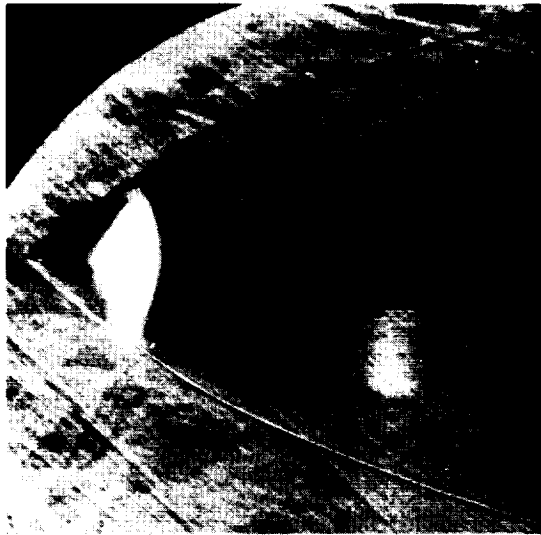
(a) Liquid-nitrogen injection; maximum penetration; high liquid-nitrogen pressure.
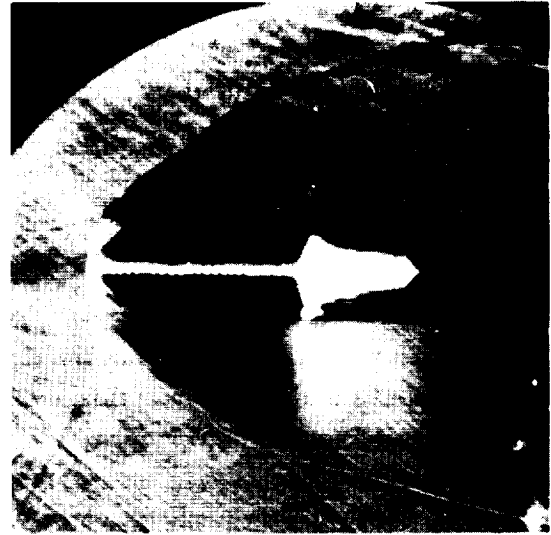
(b) Liquid-nitrogen injection; minimum penetration; high liquid-nitrogen pressure.

(c) Ambient-temperature-water injection; maximum penetration; low water pressure.

Figure 2.- Typical schlieren photographs of stagnation-point liquid injection; M = 8.   L-67-6633

generally extended some small distance away from the orifice during the ambient-temperature water-injection tests, but during the liquid-nitrogen and heated-water tests the jet appeared to break up into a droplet spray at the orifice exit. These differences are presumably caused mainly by the differences in liquid vapor pressure between the various sets of data.

8

Another difference between the results with liquid nitrogen and those with water is apparent from the photographs of figure 2, which show that the bow shock in the vicinity of the shoulder is displaced much farther out from the body for the liquid-nitrogen injection than for the water injection. This greater displacement was probably caused partly by the more rapid breakup of the liquid-nitrogen jet but mostly by the greater evaporation rates of the liquid-nitrogen droplets at the wind-tunnel conditions of the present tests. This aspect of the test data is discussed in more detail in the next section.

Penetration

To determine the mechanism that causes the large forward penetrations observed in these tests, a simplified approach was used that is particularly applicable to the ambient-temperature water injection. The procedure is described in the following paragraphs.

Assume that the liquid jet is broken up by the airstream and by internal forces (surface tension and vapor pressure) into a series of small drops which are approximately spherical. They are characterized by a radius L, the radius of the largest drops formed in the initial jet breakup. As a first-order approximation, the only aerodynamic force acting on the characteristic element is the drag force:

$$F_D = C_D \frac{\rho_\infty V_\infty^2}{2} \pi L^2 \tag{1}$$

where the drag coefficient C_D is defined in terms of the stream momentum flux and V_∞ is assumed to be much larger than V_l. The deceleration of a liquid drop is then given by

$$-C_D \frac{\rho_\infty V_\infty^2}{2} \pi L^2 = \rho_l \frac{4}{3} \pi L^3 \frac{dx^2}{dt^2} \tag{2}$$

where it has been assumed that the mass and mean dimension of the element will remain a constant. The x-coordinate has a direction counter to the airstream and its origin is assumed to be at the exit of the injection orifice. That, in general, the penetration is due to the motion of liquid particles rather than a coherent jet of liquid is shown in figure 3 by a typical schlieren photograph. Although there is a short length of coherent jet, fluid particles are in evidence over most of the penetration length. Hence, the breakup distance of the liquid jet is neglected in the following analysis. Integration of equation (2) results in

$$x = -\int \left[\int \frac{3C_D \rho_\infty V_\infty^2}{8 L \rho_l} dt \right] dt + C_1 \int dt + C_2 \tag{2a}$$

9

The initial conditions for equation (2) are: at $t = 0$, $x = 0$, and $dx/dt = V_l$. Solving for δ_2 (the value of x where $dx/dt = 0$) then gives

$$\delta_2 = \frac{4}{3} \frac{L}{C_D} \frac{\rho_l V_l^2}{\rho_\infty V_\infty^2}$$

(3)

Therefore, with a well-behaved flow of air in the vicinity of the liquid particles and no evaporation, the maximum liquid penetration would be given by equation (3), if the largest particle size were used.
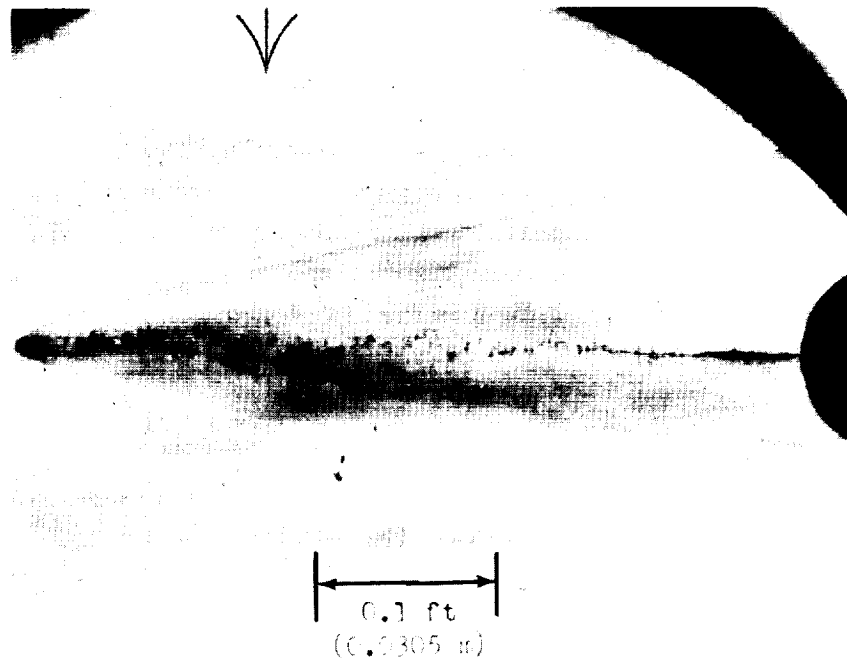
Figure 3.- Schlieren photograph showing particles of liquid after jet breakup. Ambient-temperature-water injection; M = 8; high water pressure.   L-67-6634

For the test shown in figure 3, the ratio $\rho_l V_l^2/\rho_\infty V_\infty^2$ was 26.8. A measured value of L, 0.006 ft (0.0018 m), is representative of the maximum-size particles observed in figure 3. If C_D is assumed to be 1, the δ_2 value calculated from equation (3) is then 0.214 ft (0.0652 m). While this value is of the correct order of magnitude, it is smaller by more than 0.1 ft (0.03 m) than the actual penetration shown in figure 3 if the length of the coherent jet is subtracted from δ_{tot}. This additional penetration beyond the computed value is believed to be due to a separated flow region caused by the liquid injection. In figure 4, shocks which are presumably caused by the separated flow region can be seen within the flow field ahead of the test model and downstream of the main bow

10
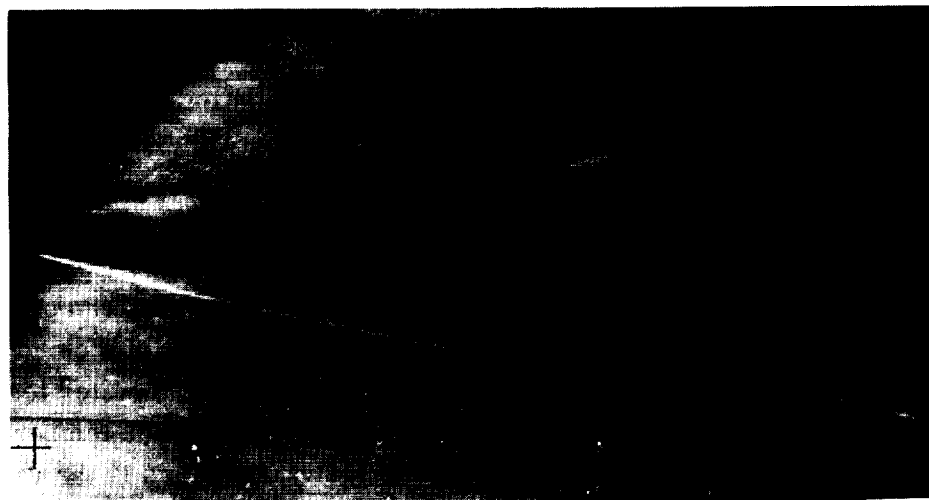
Figure 4.- Schlieren photographs showing embedded shocks from separated flow region caused by   L-67-6635
liquid injection. Ambient-temperature-water injection; M = 8; high water pressure.

shock.   This separated flow region severely complicates the analysis of the liquid-drop
trajectories, since during the passage of the drops through the recirculating separated
flow region, the drag on them is reduced.   That is, the upstream penetration of the liquid
drops creates a drag-reduction mechanism (flow separation), which allows the particles
to penetrate farther than would be the case for no separation.   Separated flow regions of
this type have been found to be oscillatory (ref. 8), and therefore it is not surprising that

the δ_{tot} value was found to oscillate in the present tests. A possible alternative explanation for the observed flow oscillation is the fact that the liquid particles which penetrate to form the maximum forward extent of the shock system probably interact with each other and therefore do not all have the same velocity in the x-direction. As the penetration is proportional to the velocity, particles arriving in the vicinity of the vortex with varying velocity would cause a varying penetration.

Although there is no direct evidence of a separated flow region for the liquid-nitrogen injection data (typified by figs. 2(a) and 2(b)), the conical bow shock of about 40° half-angle in figure 2(a) dictates that the airflow must turn through an angle of approximately 30° and thus will not impinge on the model. The region in front of the model therefore consists primarily of a conical separated flow region which is supported by the evaporating injectant. Most of the interior flow is derived from the evaporated liquid and instead of recirculating, passes downstream over the shoulder of the body as a gas. The mechanisms involved are discussed in appendix A.

Because of this separated flow region, the integration which leads to equation (3) must be carried out from the end of the separated region instead of from the orifice exit (assuming no deceleration in the separated region). Therefore, the actual δ_{tot} measured will be larger than the value obtained from equation (3); that is, equation (3) should give a lower limit for the total penetration.

If equation (3) is to be used, even as a guide in correlating the data, a value of L is needed. Where values of L can be measured (in the ambient-temperature water-injection tests), the size of the largest drops is of the same order of magnitude as that of the drops in figure 3. Since during these tests the liquid velocity, stream density, and orifice diameter were varied, evidently the drop size due to initial jet breakup is not a function of these variables. However, in the heated-water tests, instead of rather large discrete drops being present, the water spray appeared to consist of a cloud of drops too small to be measured in the schlieren photographs. As the heated-water tests were conducted under the same tunnel and injection conditions as the ambient-temperature water tests, the major difference between the two sets of test parameters is the vapor pressure of the liquid.

On the basis of these observations, a maximum effective critical Weber number is defined as

$$N_{We} \equiv \frac{Lp_v}{\sigma}$$

or

$$L = \frac{N_{We}\sigma}{p_v} \tag{4}$$

12

A maximum critical Weber number is usually defined in terms of $\rho_g V_g{}^2$ instead of p_v. However, in the present case, where for all tests the jet breakup occurs in a region of low-velocity separated flow, V_g is of the order of V_l, and ρ_g is of the order of ρ_∞. Therefore, for the present case, $\rho_g V_g{}^2 \sim \rho_\infty V_l{}^2 \ll p_v$, which indicates that the major disruptive force is characterized by p_v. It is now assumed that the value of L given by equation (4) will not be appreciably affected after the drops enter the "attached" flow region; therefore equation (3) becomes

$$\delta_2 \propto \frac{\sigma}{p_v} \frac{\rho_l V_l{}^2}{\rho_\infty V_\infty{}^2} \tag{5}$$

where it is assumed that C_D is a constant. (See fig. 5 for idealized flow field.)
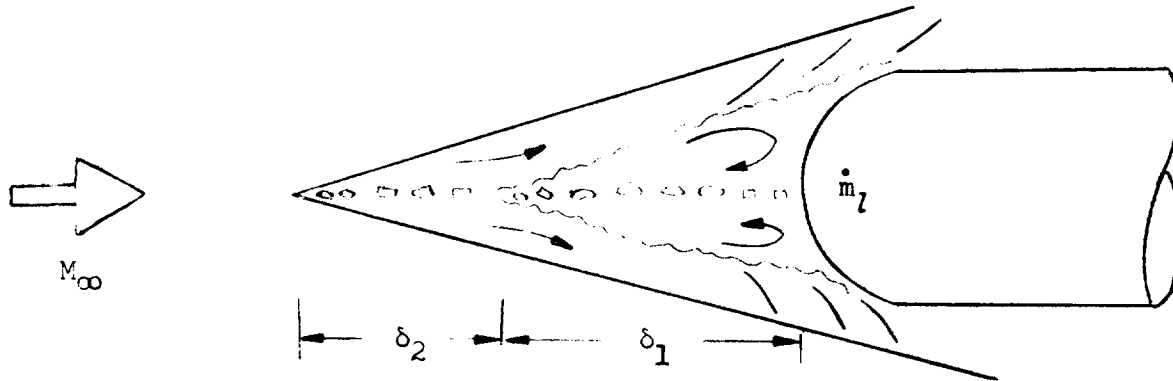
Figure 5.- Idealized flow field with injection.

It is now noted that

$$\delta_{tot} = \frac{1}{\delta_2/\delta_{tot}} \delta_2 \tag{6}$$

where δ_2/δ_{tot} is the fraction of the total penetration over which "attached" shear flow occurs. In reference 9 it is shown that for laminar flow over a flared axisymmetric body, the fraction of body length over which attached flow occurs is inversely proportional to the free-stream Reynolds number based on the body diameter.

For the present case it will be assumed that

$$\frac{\delta_2}{\delta_{tot}} \propto N_{Re}{}^{-n}$$

13

or

$$\delta_{tot} \propto N_{Re}{}^{n}\delta_2 \tag{7}$$

where n and the constant of proportionality will be determined from the present data, and δ_2 is given by expression (5).

In the preceding discussion it has been assumed that the extent of the attached flow region is primarily a function of N_{Re}. This assumption is based on data in refer-ences 10 and 11 which indicate that the effect of Reynolds number is much greater than that of the other variables involved, M_∞ and T_w/T_t. Also, negligible evaporation has been assumed; that is, the injected liquid is assumed not to evaporate in either the attached or separated flow region. This is probably a valid assumption for the case of water injection (fig. 2(c)), where the shock is not moved out appreciably in the vicinity of the shoulder of the body and the separated flow region seems to reattach on the body. However, this is not true for liquid-nitrogen injection (figs. 2(a) and 2(b)), where the lateral displacement of the body bow shock indicates that appreciable evaporation has occurred. Also, the separated flow region no longer reattaches on the model. That is, the separated region has changed from a closed, recirculating region to a mixing region where mass is added and mixes with the incoming air before passing downstream. Theo-retical calculations given in reference 12 indicate that mass injection into a base-type separated flow region appreciably increases the extent of that region. Thus, where appreciable evaporation of the injected liquid is occurring in the separated flow region, the extent of that region would be increased and therefore δ_{tot} would be increased, if all other conditions were the same and the larger particles did not undergo appreciable evaporation. Therefore expression (7) should give a minimum value of penetration because negligible evaporation was assumed in the derivation.

The following considerations can be used to ascertain some of the important param-eters which characterize the amount of mass injection that results from droplet evapora-tion for the case of liquid nitrogen. It should be noted that the mass injection occurs in the form of small contributions from many distributed sources (liquid particles), and therefore approaches such as that taken in reference 13 for upstream gas injection are not valid in the present case.

If it is assumed that the injected liquid is broken up into a number of equal-sized drops which then evaporate at a uniform rate, the ratio of evaporated liquid to incoming airflow in a stream tube of diameter D (nose diameter) is given approximately by

$$K \approx \frac{\rho_l V_l d_o{}^2}{\rho_\infty V_\infty D^2}\left(1 - R^3\right) \tag{8}$$

14

where

$$R^3 \equiv \left(\frac{r}{L}\right)^3$$

It is seen that the orifice diameter enters into expression (8), whereas it does not appear in expression (7), which gives δ_{tot} for negligible evaporation.

The rate of evaporation of the representative drop can be expressed approximately as follows:

$$\frac{dr^3}{dt}\frac{4}{3}\pi H_{f_g}\rho_2 = -\frac{4N_{Nu}\pi r^2}{r}k_{g,w,d}\left(\frac{fV_\infty^2}{2c_{p,g}} - T_{w,d}\right) \tag{9}$$

where f is the fraction of free-stream total enthalpy which exists in the separated region. Since $dx/dt = V$ in the separated region, equation (9) becomes

$$\frac{dr^2}{dx} \propto -\frac{N_{Nu}}{V_l}\frac{k_{g,w,d}}{H_{f_g}\rho_l}\left(\frac{fV_\infty^2}{2c_{p,g}} - T_{w,d}\right) \tag{10}$$

where it has been assumed that all of the heat transferred to the drop is used for evaporation of the liquid. Since the initial drop size can again be characterized by equation (4), the above expression becomes

$$\frac{dR^2}{dx} \propto -\frac{N_{Nu}}{V_l}\frac{k_{g,w,d}}{H_{f_g}\rho_l}\left(\frac{p_v}{\sigma}\right)^2\left(\frac{fV_\infty^2}{2c_{p,g}} - T_{w,d}\right) \tag{11}$$

To calculate a K value from expression (8) it would be necessary to integrate expression (11). However, the relative amounts of evaporation to be expected from water and liquid nitrogen can be obtained qualitatively by an inspection of the expression for dR^2/dx, which is proportional to the rate of evaporation.

The quantity $k_{g,w,d}/H_{f_g}(p_v/\sigma)^2$ is of the order of 10^3 times greater for the liquid-nitrogen injection tests than for the water tests, and therefore much more evaporation should occur for the liquid-nitrogen injection tests. (That this is indeed the case is indicated qualitatively by comparison of figures 2(a) and 2(c).) The other terms in expression (11) are of the same order of magnitude for both sets of data.

It is therefore apparent that, while the functional dependencies for δ_{tot} can be found if evaporation is negligible (expression (7)) and a satisfactory expression for δ_{tot} can be ascertained for this condition, the case in which evaporation occurs is much more complicated. Because of the large number of variables involved and the fact that they would not appear as simple multiplying factors (i.e., contributions to δ_{tot} due to evaporation would have to approach zero as $R^3 \to 1$) as well as the lack of applicable data, it is not possible at the present time to obtain an expression which applies in the regime between essentially no evaporation (water injection) and almost complete evaporation with relatively large liquid mass flows (liquid-nitrogen injection). A simplified method which is used to obtain an order-of-magnitude determination of the effect of evaporation for the case in which evaporation is the dominant effect is given in appendix A.

The results of the application of expression (7) to the data are shown in figure 6. The nominal test conditions for each set of data are given in the figure, and actual values of the parameters are given in table I. Included in figure 6 as corroborating information are unpublished data obtained at Mach numbers of 6 and 17.5 by other investigators. (Details concerning these data are given in appendix B.) To show the amount of scatter in the data, dashed lines indicating ±50 percent from each of the correlating lines have been shown. There is no consistent scatter at any one set of conditions; that is, the high Mach number data appear on both sides of the correlating line, as do the lower Mach number data. In view of the complicated flow mechanisms involved (liquid-jet atomization, evaporation of liquid, momentum interchange between liquid particles and airstream, and flow separation), the wide range of test conditions represented by the data, and the remarks made in the accuracy section, the scatter shown is considered acceptable.

It is apparent from figure 6 that the simple approach taken herein (expression (7)) can be used to formulate an empirical expression for the amount of penetration for stagnation-point injection when little evaporation occurs (water injection). For this case the correlating line shown has the equation

$$\frac{\delta_{tot} p_v}{c} = 2.25 \frac{\rho_l V_l^2}{\rho_\infty V_\infty^2} \left(\frac{\rho_\infty V_\infty D}{\mu_\infty} \right)^{0.4} \tag{12}$$

It is surprising that the orifice diameter d_o does not appear in equation (12). Since d_o was varied by a factor of 10, and no effect on penetration was observed, it can be concluded that the forward penetration is not a function of orifice diameter for the case of negligible evaporation. Therefore, to obtain a desired penetration it is only necessary to have the correct value of V_l, and the liquid mass flow may be made as small as practicable. This conclusion that δ_{tot} is independent of d_o is at odds with the conclusion in reference 3 for cross-stream injection in subsonic flows, where δ_{tot} was found to be proportional to $d_o^{0.78}$.
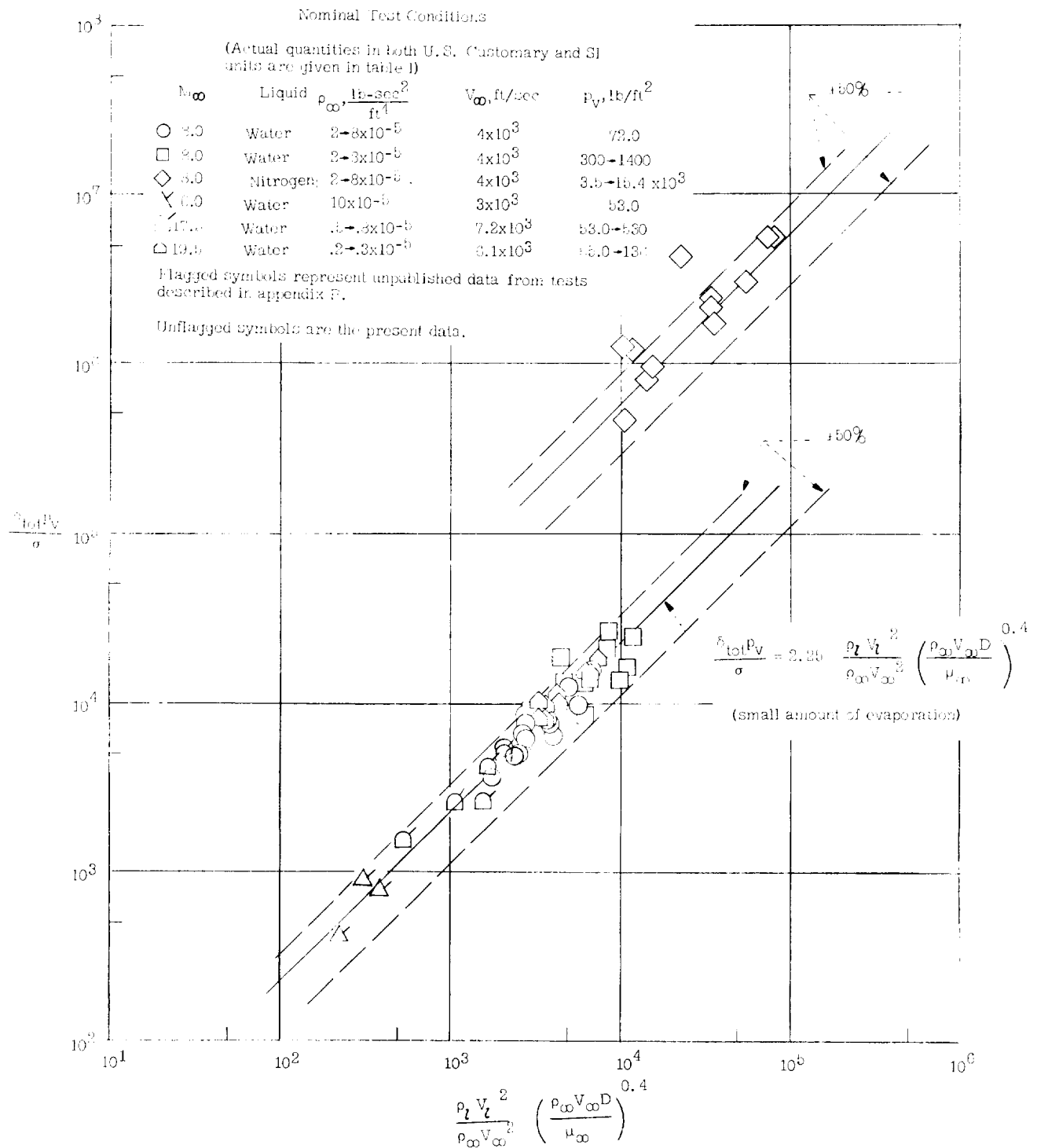
16

Figure 6.- Correlation of maximum forward penetration for stagnation-point liquid injection.

The data from the liquid-nitrogen tests are also plotted in figure 6, and it is apparent (as would be expected from the previous discussion) that the parameters used here do not correlate these data with the water injection data. Although the liquid-nitrogen data are self-correlated fairly satisfactorily by the parameters of figure 6 (from expression (7)), the agreement may be fortuitous because the range of test conditions is small. However, as stated previously, a simplified method for obtaining the order of magnitude of the effect of a fairly large amount of evaporation (more than 50 percent) is given in appendix A. It should again be pointed out that with appreciable evaporation the "separated flow" region is now a flow field where mass is added. This mass has to pass downstream at the model shoulder, so a closed recirculatory region cannot be assumed. The final expression obtained is given as equation (A14) in appendix A.

Shown in figure 7 are the results of the application of equation (A14) to the liquid-nitrogen data. The data scatter is somewhat less than for the liquid-nitrogen results shown in figure 6, as would be expected if the primary effect is one of evaporation rather than one of penetration of liquid particles. The data where $\delta_{tot} \leqq D/2$ $(D/2 = 0.06$ ft or 0.0183 m) show more scatter, which is reasonable as the assumption of $\delta_{tot} > D/2$ was made in the derivation of equation (A14). The resulting expression is:

$$\frac{\left(\delta_{tot} + \frac{D}{2}\right)\rho_\infty V_\infty^2}{\sqrt{\rho_\infty V_\infty \rho_l V_l d_o^2 \left(1 - R^3\right)\left(\frac{V_\infty^2}{2} + c_{p,V} T_V - H_{f_g}\right)}} = 1.4 \tag{13}$$

As a result of assumptions made in the derivation of equation (A14) (see appendix A), its use is restricted to cases where $V_l \ll V_\infty$, $d_o \ll \delta_{tot}$, $\delta_{tot} > D/2$, and bow shock half-angles are about 40°. If more than one orifice of the same size is used, the number of orifices will appear as a factor within the square-root expression. Equation (13) indicates that for the case where evaporation is dominant, δ_{tot} is proportional to d_o.

Because of the large number of variables involved when evaporation of the injectant takes place in the separated flow region, and because most of the data for liquid-nitrogen injection represent a large amount of evaporation, it was not possible to obtain a correlation which included the effects of moderate amounts of evaporation.

Equation (12) can, however, be used to obtain a lower limit of the penetration if evaporation is slight. A design based on this lower limit would probably insure the success of an experiment using water injection to provide aerodynamic shaping to relieve signal blackout (ref. 1), as overpenetration caused by small amounts of evaporation would lead to a further reduction in postshock free-electron concentration (assuming that the larger particles, which cause the maximum penetration, are not reduced greatly in size by evaporation).

18

$$\frac{\left[\rho_\infty V_\infty \rho_l V_l d_o{}^2 (1 - R^3)\left(\frac{V_\infty{}^2}{2} + c_{p,v} T_v - H_{f_g}\right)\right]^{1/2}}{\rho_\infty V_\infty{}^2}$$
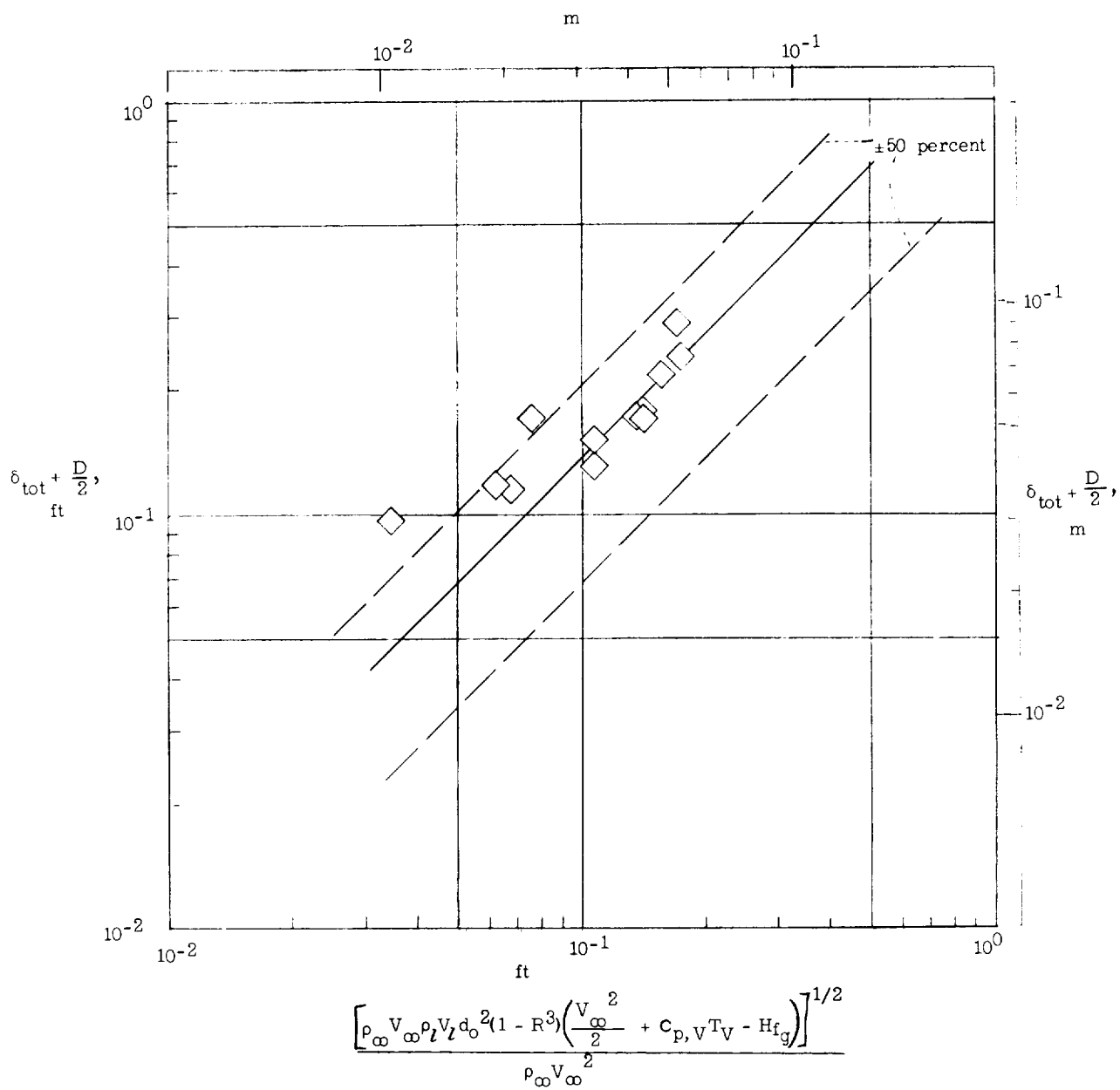
Figure 7.- Correlation of liquid-nitrogen injection data on the basis of the evaporation parameter (eq. (A14)).

19

The RAM B2 flight vehicle was a spherically blunted 9° half-angle cone with an 8-inch (20.3-cm) nose diameter. A detailed description of the vehicle and the flight trajectory are given in reference 14. The primary purpose of the flight test was to measure the effect of water injection on radio transmission from the vehicle. During periods of no water injection the radio transmission was completely blacked out by the large concentration of free electrons in the flow field, but the injection of water from the stagnation region during the flight test resulted in appreciable radio-signal recovery (ref. 1). In the present report consideration will be given only to the periods during stagnation-region injection when a single orifice was used.

If the forward penetration of the water during injection from the stagnation region was sufficient to change the bow shock to a pointed shape, signal recovery would be expected because of the reduction in electron concentration. That is, the free-electron concentration behind such a pointed shock would be much less than behind a normal undisturbed bow shock, and possibly low enough to permit signal recovery (the assumption here is that most of the free electrons are produced in the normal-shock region rather than in the viscous boundary layer). To check this hypothesis, the penetration for stagnation-region injection was calculated for the RAM B2 flight trajectory conditions. The amount of evaporation that would occur during the flight was estimated by integrating equation (9) for $f = 0.8$, a penetration distance of 0.4 ft (0.122 m), and $N_{Nu} = 2$. The resulting values were less than 10 percent (i.e., $R^3 \geqq 0.9$) and therefore equation (12) is directly applicable. The nominal water temperature was taken as 80° F (300° K). Values of liquid velocity obtained from flight-test data and corresponding values of δ_{tot} as computed from equation (12) are given in the following table, along with the flight velocity and altitude:

Altitude		V_∞		V_l		δ_{tot} (from eq. (12))	
ft	m	ft/sec	m/sec	ft/sec	m/sec	ft	m
150×10^3	45.7×10^3	15.4×10^3	4.69×10^3	130	39.6	0.615	0.187
160	48.7	17.85	5.44	105	32.0	.4	.122
170	51.8	17.8	5.42	87	26.5	.347	.106
180	54.8	17.75	5.4	80	24.4	.354	.108
190	57.9	17.70	5.39	70	21.3	.345	.105
200	60.9	17.65	5.38	64	19.5	.374	.114
210	64.0	17.60	5.36	60	18.3	.408	.124

A value of δ_{tot} of about 0.6 ft (0.183 m) for this vehicle would result in a conical shock with a half-angle of about 25° in the type of flow field observed in the present wind-tunnel investigation for negligible evaporation. Calculations of electron concentration behind a shock with this angle show that the free-electron concentration in the inviscid flow field is reduced below critical values for radio transmission (ref. 1). Since the δ_{tot} values with the small amount of evaporation which occurred are probably on the order of 0.6 ft (0.0183 m), the observed signal recovery may have been due primarily to flow-field shaping caused by forward liquid penetration for the period when a single orifice was used. Further details and an analysis of the RAM B2 flight are given in reference 15.

SUMMARY OF RESULTS

The maximum forward penetration of liquid water and liquid nitrogen injected from the stagnation point of a hemispherically blunted body has been measured at Mach numbers of 8 and 19.5. The following results were obtained:

1. The extent of the penetration was found to oscillate during a given test. For water injection the bow shock always had a pointed shape during these oscillations, whereas for liquid-nitrogen injection the bow shock was pointed for maximum penetration but fairly blunt for minimum penetration. These oscillations appeared to be due to the existence of a separated flow region caused by the liquid injection.

2. For the no-evaporation case an expression based on an analysis was obtained for the maximum forward extent of the penetration as a function of free-stream density, velocity, and viscosity, liquid density and velocity, liquid vapor pressure and surface tension, and model nose diameter.

3. For the case in which evaporation is the dominant mechanism affecting penetration, the data were correlated on the basis of a parameter from a simplified analysis which included model diameter, free-stream density and velocity, liquid density and velocity, orifice diameter, percent of evaporation, and latent heat of the liquid.

4. The maximum forward penetration was found to be independent of the injection-orifice diameter for the case of negligible liquid evaporation.

Langley Research Center,
    National Aeronautics and Space Administration,
        Langley Station, Hampton, Va., May 2, 1967,
            125-21-02-09-23.

APPENDIX A

APPROXIMATE METHOD OF OBTAINING THE EFFECT OF EVAPORATION ON THE FORWARD PENETRATION OF INJECTED LIQUIDS

The purpose of this appendix is to present a simplified approach to the problem of determining the effect of evaporation on the forward penetration of liquids injected from the stagnation point of a blunt body.

Consider the idealized flow field shown in figure 8. This flow model is based on the observed fact that for the liquid-nitrogen data the shock angle θ was approximately independent of the amount of penetration and the bow shock was conical in shape for maximum penetration. The evaporation of the injected liquid is assumed to cause a certain amount of penetration δ_{tot} (equal to $a + b$). The airflow is assumed to be turned through an angle α by the bow shock and it is assumed that a region of mixing between air and injectant occurs along an angle ψ, equal to the cone half-angle corresponding to the shock-wave angle θ. The control volume bounded by the "boundary streamline" shown is used to write the one-dimensional conservation equations. Because a large percentage of evaporation is assumed, the drops will be too small to penetrate beyond the "separated flow" region, and therefore $\delta_{tot} = \delta_1$ in the present case. It is assumed that the liquid is injected from the stagnation point at a flow rate $\dot{m}_l$.

For one-dimensional flow, conservation of mass requires that (for a single orifice):

$$\rho_\infty V_\infty \pi \bar{r}^2 + \rho_l V_l \pi \frac{d_o^2}{4}\left(1 - R^3\right) = \rho_{av} V_{av} \pi \left[\left(h + \frac{D}{2}\right)^2 - \left(\frac{D}{2}\right)^2\right] \tag{A1}$$

where the subscript av refers to average gas-mixture quantities at the body shoulder, and R is the ratio of the mean drop radius at the body shoulder to the initial drop radius.

The equation for conservation of momentum in the x-direction is

$$p_{av}\left[\left(h + \frac{D}{2}\right)^2 - \bar{r}^2\right]\pi + p_\infty \pi \bar{r}^2 + \rho_\infty V_\infty^2 \pi \bar{r} = \pi p_{av}\left[\left(h + \frac{D}{2}\right)^2 - \left(\frac{D}{2}\right)^2\right]$$

$$+ \rho_{av} V_{av}^2 \pi \left[\left(h + \frac{D}{2}\right)^2 - \left(\frac{D}{2}\right)^2\right] + p_{av}\pi \frac{D^2}{4} + \rho_l V_l^2 \pi \frac{d_o^2}{4} \tag{A2}$$

where the momentum of the liquid still present at the shoulder has been neglected.
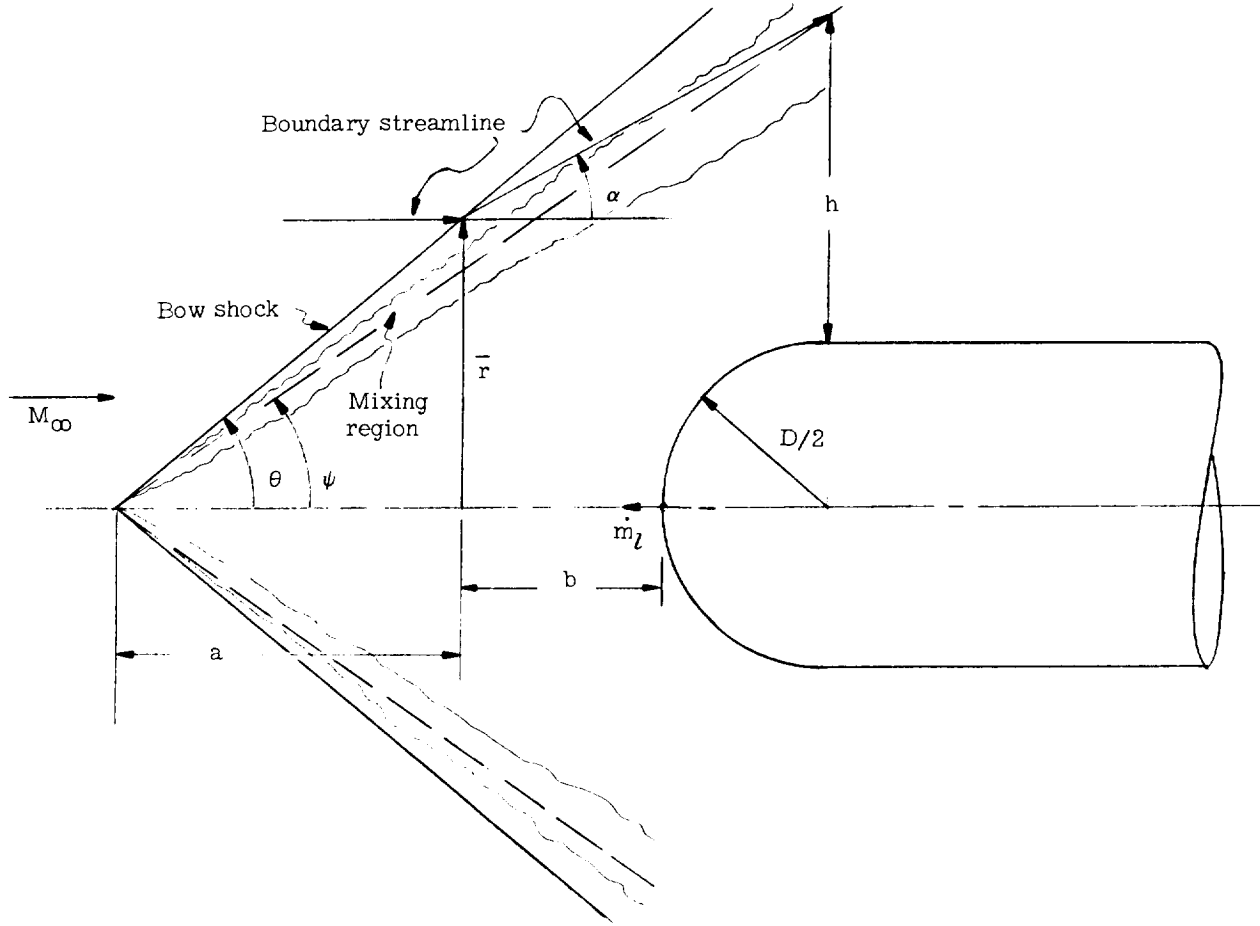
Figure 8.- Idealized flow field used to obtain approximate effect of evaporation upon penetration.

Conservation of energy requires that

$$\frac{V_\infty^2}{2}\rho_\infty V_\infty \pi \bar{r}^2 - \rho_l V_l \frac{\pi d_o^2}{4}\left(1 - R^3\right)\left(H_{f_g} - c_{p,V}T_V\right) = \rho_{av}V_{av}\pi\left[\left(h + \frac{D}{2}\right)^2\right.$$

$$\left. - \left(\frac{D}{2}\right)^2\right]\left(c_pT_{av} + \frac{V_{av}^2}{2}\right) \tag{A3}$$

Also,

$$\rho_{av} = \frac{p_{av}}{\bar{R}T_{av}} \tag{A4}$$

23

where p_{av} is assumed to be equal to the static pressure behind a shock with an angle θ (diffusion of momentum and energy across the boundary streamline have been neglected). From figure 8, some required geometric relations are obtained:

$$a + b = \delta_{tot} \tag{A5}$$

$$\tan \psi = \frac{h + \dfrac{D}{2}}{\delta_{tot} + \dfrac{D}{2}} \tag{A6}$$

$$\tan \theta = \frac{\bar{r}}{a} \tag{A7}$$

$$\tan \alpha = \frac{h + \dfrac{D}{2} - \bar{r}}{b + \dfrac{D}{2}} \tag{A8}$$

where α is equal to the two-dimensional-flow turning angle for the shock with angle θ. Therefore,

$$h = \left(\delta_{tot} + \frac{D}{2}\right)\tan \psi - \frac{D}{2} \tag{A9}$$

and

$$\bar{r} = \left[\frac{\tan \theta}{1 - \dfrac{\tan \theta}{\tan \alpha}}\left(1 - \frac{\tan \psi}{\tan \alpha}\right)\right]\left(\delta_{tot} + \frac{D}{2}\right) \tag{A10}$$

For a given θ, the quantity in brackets is a constant, and therefore equations are available for $\bar{r}$ and h in terms of δ_{tot}. The solution to equations (A1), (A2), and (A3) with unknowns δ_{tot}, T_{av}, and V_{av} can then be obtained in terms of δ_{tot} if the values of θ and R^3 are known.

Eliminating the variables T_{av} and V_{av} from equations (A1), (A2), and (A3) and using the relations (A4) and (A9) gives the following equation (after dividing each term by $d_0{}^4 \rho_\infty{}^2 V_\infty{}^4$):

24

$$- \frac{\rho_l^2 V_l^4}{16\rho_\infty^2 V_\infty^4} - \frac{\rho_l^2 V_l^2 \left(1 - R^3\right)^2 H_{fg}}{16\rho_\infty^2 V_\infty^4} + \frac{\rho_l^2 V_l^2 c_{p,V} T_V \left(1 - R^3\right)^2}{16\rho_\infty^2 V_\infty^4} - \frac{p_{av} \bar{r}^2 \rho_l V_l^2}{2d_o^2 \rho_\infty^2 V_\infty^4} + \frac{\bar{r}^2 \rho_l V_l^2}{2d_o^2 \rho_\infty V_\infty^2}$$

$$+ \frac{\rho_l V_l^2 c_p A p_{av}}{4\bar{R} d_o^2 \rho_\infty^2 V_\infty^4} + \frac{\rho_l V_l \left(1 - R^3\right) \bar{r}^2}{8d_o^2 \rho_\infty V_\infty} - \frac{\bar{r}^2 H_{fg} \left(1 - R^3\right) \rho_l V_l}{4\rho_\infty V_\infty^3 d_o^2} + \frac{\bar{r}^2 \left(1 - R^3\right) c_{p,V} T_V \rho_l V_l}{4d_o^2 \rho_\infty V_\infty^3}$$

$$- \frac{p_{av}^2 \bar{r}^4}{d_o^4 \rho_\infty^2 V_\infty^4} + \frac{2p_{av} \bar{r}^4}{d_o^4 \rho_\infty V_\infty^2} - \frac{\bar{r}^4}{d_o^4} + \frac{\bar{r}^2 c_p A p_{av}^2}{\bar{R} d_o^4 \rho_\infty^2 V_\infty^4} - \frac{c_p A p_{av} \bar{r}^2}{\bar{R} \rho_\infty V_\infty^2 d_o^4} + \frac{\bar{r}^4}{2d_o^4} = 0 \qquad \text{(A11)}$$

where

$$A = \left(\delta_{tot} + \frac{D}{2}\right)^2 \tan^2\psi - \frac{D^2}{4} \qquad \text{(A12)}$$

In order to obtain a simple expression in terms of the quantity $\delta_{tot} + \frac{D}{2}$, it is assumed that A is of the order of $\left(\delta_{tot} + \frac{D}{2}\right)^2$, which is reasonable for $\delta_{tot} > \frac{D}{2}$.

If, as is true of the present data, d_o is much smaller than δ_{tot}, terms of order $\rho_l^2 V_l^4 / \rho_\infty^2 V_\infty^4$ are negligible with respect to terms of order $\bar{r}^4 / d_o^4$ and $\rho_l V_l^2 \bar{r}^2 / \rho_\infty V_\infty^2 d_o^2$. Thus the first three terms of equation (A11) can be dropped. Also, when $V_l \ll V_\infty$ and $R^3 < 0.5$, the fourth, fifth, and sixth terms, which contain a $\left(\delta_{tot} + \frac{D}{2}\right)^2$ factor, are negligible with respect to the seventh, eighth, and ninth terms, which are the other terms that contain a $\left(\sigma_{tot} + \frac{D}{2}\right)^2$ factor.

Therefore equation (A11) reduces to:

$$\left(\delta_{tot} + \frac{D}{2}\right)^4 \rho_\infty^2 V_\infty^4 \approx (\text{Constant}) \left(\delta_{tot} + \frac{D}{2}\right)^2 \left(\rho_\infty V_\infty \rho_l V_l \frac{d_o^2}{4}\right) \left(1 - R^3\right) \left(c_{p,V} T_V + \frac{V_\infty^2}{2} - H_{fg}\right)$$

$$\text{(A13)}$$

or

$$\delta_{tot} + \frac{D}{2} \propto \frac{\sqrt{\rho_\infty V_\infty \rho_l V_l d_o{}^2 \left(1 - R^3\right)\left(\frac{V_\infty{}^2}{2} + c_{p,V} T_V - Hf_g\right)}}{\rho_\infty V_\infty{}^2} \tag{A14}$$

There is an $N_{Re}{}^{0.4}$ effect on δ_{tot}, according to figure 6; however, as the extent of the separated region is expected to be dictated primarily by the amount of mass addition for $R^3 \rightarrow 0$, and the correct variation of ρ_∞ (one of the principal quantities varied during the present tests) is already included in equation (A14), the effect of N_{Re} is assumed to be negligible.

The constant of proportionality for equation (A14) can be obtained from the data for the present liquid-nitrogen tests, where appreciable evaporation occurred. However, the applicability of the resulting expression to conditions much different from those of the present tests is dubious, mainly because the proportionality constant is a function of the shock angle that occurs. For the present liquid-nitrogen injection tests, this angle is approximately 37°. Also, there are no gas-chemistry effects in the present case. If these chemistry effects were present, they would change the value of the shock angle. However, equation (A14) should give the correct order of magnitude of the effect of evaporation of the injectant on penetration for large amounts of evaporation.

The value of R^3 needed to obtain the proportionality constant can be obtained from an integration of the rate equation (eq. (9)). Assuming the average-size particle to be given by equation (4), where $W = 88.6$ as evaluated from the data shown in figure 3, and using a distance for integration of 0.1 ft, gives a value of $R^3 \approx 0$ for the liquid-nitrogen injection data (assuming $f = 0.8$ and $N_{Nu} = 2$). Because some liquid was still observed aft of the shoulder during the tests, as indicated by the light beam about 2 diameters downstream of the model nose in figure 2(a), the value of R^3 to be used in obtaining the constant will be 0.2. However, this will not make a great deal of difference in the final value of the proportionality constant for equation (A14). The results of the application of equation (A14) to the data are presented in the body of the present paper.

APPENDIX B

SUMMARY OF UNPUBLISHED TESTS OF STAGNATION-POINT
WATER INJECTION AT MACH NUMBERS OF 6 AND 17.5

A limited number of measurements of the maximum penetration for stagnation-point water injection have been obtained at Mach numbers of 6 and 17.5. The purpose of this appendix is to give a summary of the test conditions under which these measurements were made.

Facilities

The Mach 6 tests were carried out by William L. Weaver and William F. Henson in the Langley 20-inch Mach 6 tunnel, which is an intermittent tunnel that exhausts to atmosphere with the aid of a supersonic annular ejector. Nominal operating conditions were a stagnation temperature of 500° F (533° K) and a stagnation pressure of 215 psia (1.48×10^6 N/m^2). Further details concerning the facility are available in reference 16.

The Mach 17.5 tests were conducted in the LTV hypervelocity wind tunnel under contract to Langley Research Center and were monitored by William L. Weaver of Langley. This facility is an arc-heated "hotshot" type of blowdown tunnel with a variable-volume arc chamber. Nominal operating conditions for the facility were a stagnation pressure of 5000 psia (3.45×10^7 N/m^2) and a stagnation temperature of 4540° F (2777° K). Further information concerning the facility is available in reference 17. Actual values of free-stream properties for both sets of tests are given in table I.

Models

The basic configuration used was a spherically blunted 9° half-angle cone. The nose diameter of the model is given in table I for each set of tests, as is the range of orifice diameters used. All orifices had essentially a 90° entrance condition. Given in table II are the l/d_0 values for these orifices. All tests were carried out with a single orifice mounted at the stagnation point, except for one case (noted in table I) in which nine orifices were used.

Test Procedures and Data Reduction

The test procedures were similar to those used in the investigation described in the body of the paper. All tests were carried out with ambient-temperature water, except for one test at $M = 17.5$ where the water was heated to 150° F (339° K). In the Mach 6 tests the maximum penetration was determined from a limited number of schlieren pictures; therefore the remarks in the section entitled "Accuracy" in the body

of this report are also applicable to these data. High-speed motion pictures were made of the flow field during the Mach 17.5 tests, and therefore the maximum penetration observed should be correct, except as modified by possible small nonsteady-state effects in the water system due to the short test time (200 msec) of the tunnel.

REFERENCES

1. Huber, Paul W.; and Sims, Theo E.: The Entry-Communications Problem. Astronaut. Aeron., vol. 2, no. 10, Oct. 1964, pp. 30-40.

2. Rashis, Bernard: Preliminary Indications of the Cooling Achieved by Ejecting Water Upstream From the Stagnation Point of Hemispherical, 80° Conical, and Flat-Faced Nose Shapes at a Stagnation Temperature of $4,000^{\circ}$ F. NACA RM L57I03, 1957.

3. Chelko, Louis J.: Penetration of Liquid Jets Into a High-Velocity Air Stream. NACA RM E50F21, 1950.

4. Szpiro, Edward J.: Secondary Fluid Injection Into a Supersonic Airstream. Rept. No. 65-2, Mech. Eng. Res. Labs., McGill Univ., Apr. 1965.

5. Beckwith, Ivan E.; and Huffman, Jarrett K.: Injection and Distribution of Liquids in the Flow Fields of Blunt Shapes at Hypersonic Speeds. NASA TM X-989, 1964.

6. Stainback, P. Calvin: Heat Transfer Measurements at a Mach Number of 8 in the Vicinity of a 90° Interior Corner Alined With the Free-Stream Velocity. NASA TN D-2417, 1964.

7. Clark, Frank L.; and Johnson, Charles B.: Real-Gas Hypersonic-Nozzle Flow Parameters for Nitrogen in Thermodynamic Equilibrium. NASA TN D-2019, 1963.

8. Bogdonoff, Seymour M.; and Vas, Irwin E.: Preliminary Investigations of Spiked Bodies at Hypersonic Speeds. J. Aero/Space Sci., vol. 26, no. 2, Feb. 1959, pp. 65-74.

9. Becker, John V.; and Korycinski, Peter F.: Heat Transfer and Pressure Distribution at a Mach Number of 6.8 on Bodies With Conical Flares and Extensive Flow Separation. NASA TN D-1260, 1962.

10. Miller, D. S.; Hijman, R.; and Childs, M. E.: Mach 8 to 22 Studies of Flow Separations Due to Deflected Control Surfaces. AIAA J., vol. 2, no. 2, Feb. 1964, pp. 312-321.

11. Johnson, Charles B.: Pressure and Flow-Field Study at Mach Number 8 of Flow Separation on a Flat Plate With Deflected Trailing-Edge Flap. NASA TN D-4308, 1968.

12. Baum, Eric; King, Hartley H.; and Denison, M. Richard: Recent Studies of the Laminar Base-Flow Region. AIAA J., vol. 2, no. 9, Sept. 1964, pp. 1527-1534.

13. Romeo, David J.; and Sterrett, James R.: Flow Field for Sonic Jet Exhausting Counter to a Hypersonic Mainstream. AIAA J. (Tech. Notes), vol. 3, no. 3, Mar. 1965, pp. 544-546.

14. Raper, James L.; Keynton, Robert J.; and Woodbury, Gerard E.: Detailed Description and Flight Performance of the RAM B Vehicle. NASA TN D-2437, 1964.

15. Cuddihy, William F.; Beckwith, Ivan E.; and Schroeder, Lyle C.: Flight Test and Analysis of a Method for Reducing Radio Attenuation During Hypersonic Flight. NASA TM X-1331, 1967.

16. Schaefer, William T., Jr.: Characteristics of Major Active Wind Tunnels at the Langley Research Center. NASA TM X-1130, 1965.

17. Stalmach, C. J., Jr.: Design and Operation of a Variable-Volume Arc Chamber in a Hypervelocity Wind Tunnel. Fourth Hypervelocity Techniques Symposium, Univ. of Denver and Arnold Eng. Develop. Center, Nov. 1965, pp. 528-570.

TABLE I.- TEST CONDITIONS

(a) U.S. Customary Units

δ, ft	d_o, ft	ρ_l, lb-sec²/ft⁴	V_l, ft/sec	p_v, lb/ft²	σ, lb/ft	ρ_∞, lb-sec²/ft⁴	V_∞, ft/sec	μ_∞, lb-sec/ft²	D, ft	M_∞	H_{fg}, ft²/sec²
Mach 8 tests — liquid-nitrogen injection											
0.0576	0.0033	1.417	218.7	9 630.0	0.000434	8.0 $\times 10^{-5}$	3970	0.76 $\times 10^{-7}$	0.1198	7.95	0.195 $\times 10^7$
.1105		1.348	331.5	15 410.0	.000397	8.04	3975			7.95	
.1588		1.429	332.0	8 390.0	.000443	1.929	3890			7.80	
.1105		1.419	256.7	9 560.0	.000434	1.94	3875				
.2305		1.406	370.4	10 296.0	.000426	1.86	3911				
.0713		1.525	137.1	3 585.0	.000544	1.84	3932				
.090		1.468	143.2	6 435.0	.000474	1.89	3883				
.179		1.373	393.8	13 130.0	.000404	1.83	3946				
.1106	.0016	1.43	251.7	8 710.0	.000443	1.817	3961			7.95	
.0368	.0016	1.395	269.0	11 304.0	.000418	7.79	4016			7.95	
.1152	.0033	1.461	258.0	6 840.0	.000467	1.91	3890			7.80	
.0550	.0033	1.461	253.0	6 840.0	.000467	8.01	3961			7.95	
Mach 6 tests — water injection											
0.0723	0.0080	1.94	30.3	53.0	0.00489	10.0 $\times 10^{-5}$	3030	0.84 $\times 10^{-7}$	0.15	6.00	0.250 $\times 10^8$
.0833	.0080		27.0			10.09					
a.0384	.0026		23.1			10.09					
Mach 17.5 tests — water injection											
0.476	0.0008	1.94	54.8	53.0	0.00489	0.517 $\times 10^{-5}$	7095	0.36 $\times 10^{-7}$	0.075	17.4	0.250 $\times 10^8$
.239			53.1	53.0	.00489	.861	7411	.596		17.6	
.0211			54.7	530	.00448	.721	7331	.347		17.6	
.138	.0013		33.5	53.0	.00489	.725	7279	.5		17.5	
.389	.0021		60.3	53.0	.00489	.713	7392	.5		17.5	
Mach 19.5 tests — water injection											
0.625	0.0033	1.94	53.8	78.0	0.00483	0.325 $\times 10^{-5}$	6150	0.28 $\times 10^{-7}$	0.1198	19.5	0.250 $\times 10^8$
1.36			70.8	65.6	.0049	.314					
1.15			64.4								
.6			48.4								
.535	.0016		46.8	73.0	.00487						
.36				136.0	.00475	.322					
.59				78.0	.00483	.278					
.89			62.0	82.6	.00483	.26					
.59			46.8	91.5	.00480	.211					
Mach 8 tests — ambient-temperature-water injection											
0.3667	0.0016	1.94	72.2	72.4	0.00489	4.49 $\times 10^{-5}$	3970	0.8 $\times 10^{-7}$	0.1198	7.95	0.250 $\times 10^8$
.575			99.0			8.21	4000				
.425			99.8			7.84	4050				
.517			98.3			7.73	4055				
.2408	.0008		79.0			7.72	4055				
.5275			96.7			4.33	4040				
.336			77.1			4.33	4040				
.333			99.8			7.93	4055				
1.024	.0016		130.8			4.47	4010				
.516			99.0			4.35	4040				
.332			79.0			4.33	4040				
.8675			132.4			7.61	4080				
.4467			96.7			7.64	4075				
.417			79.0			1.94	3980			7.80	
.6580			89.6			2.13	3720			7.80	
Mach 8 tests — heated-water injection											
0.127	0.0008	1.94	123.7	317.5	0.0046	4.68 $\times 10^{-5}$	3960	0.8 $\times 10^{-7}$	0.1198	7.95	0.250 $\times 10^8$
.0772			124.0	762	.0044	4.68	3960				
.0538			125.0	1096	.0043	7.84	4030				
.0812	.0016		128.0	755	.00443	4.73	3940				
.0597			125.2	1355	.00424	7.73	4060				
.0754			121.9	800.5	.00438	2.05	3880			7.80	
.1004			172.0	677	.00442	4.73	3940			7.95	
.1054			172.8	878	.00436	7.79	4060				
.0521			84.4	768	.00439	4.32	4080				
.141			172.5	766		4.31	4050				
.1198			170.0	768		7.71	4060				

[a]This test was run with nine orifices of the size shown, mounted in the vicinity of the stagnation point.

TABLE I.- TEST CONDITIONS — Concluded

(b) International System of Units

δ, m	d_0, m	ρ_l, kg/m³	V_l, m/sec	p_V, N/m²	σ, N/m	ρ_∞, kg/m³	V_∞, m/sec	μ_∞, N-sec/m²	D, m	M_∞	H_{fg}, m²/sec²
Mach 8 tests — liquid-nitrogen injection										
0.0175	0.0010	730.28	66.6	461 084	0.006332	4.12 ×10⁻²	1210	36.4×10⁻⁷	0.0365	7.95	0.181×10⁶
.0336		694.72	101.0	737 831	.005792	4.14	1212			7.95	
.0484		736.46	101.1	401 713	.006463	.994	1186			7.80	
.0336		731.31	78.2	457 733	.006332	.999	1181				
.0702		724.61	112.9	492 972	.006215	.958	1192				
.0217		785.94	41.8	171 650	.007937	.948	1198				
.0274		756.56	43.6	308 108	.006916	.974	1184				
.0545		707.60	120.0	628 664	.005894	.943	1203				
.0337		736.98	76.7	417 035	.006463	.936	1207				
.0112	.0005	718.94	81.9	541 236	.006099	4.01	1224			7.95	
.0351	.0010	752.96	78.6	327 499	.006814	.984	1186			7.80	
.0167	.0010	752.96	77.1	327 499	.006814	4.12	1207			7.95	
Mach 6 tests — water injection										
0.0220	0.0024	999.82	9.2	2 538	0.07135	5.15 ×10⁻²	920.5	40.2×10⁻⁷	0.0457	6.00	0.232×10⁷
.0253	.0024		8.2			5.20					
ᵃ.0117	.0008		7.0			5.20					
Mach 17.5 tests — water injection										
0.1451	0.0002	999.82	16.7	2 538	0.07135	0.266 ×10⁻²	2163	17.2×10⁻⁷	0.0228	17.4	0.232×10⁷
.0728			16.1	2 538	.07135	.443	2259	28.5		17.6	
.0064			16.6	25 330	.06536	.371	2234	16.6		17.6	
.0420	.0004		10.2	2 538	.07135	.373	2219	24.0		17.5	
.1186	.0006		18.3	2 538	.07135	.367	2253	24.0		17.5	
Mach 19.5 tests — water injection										
0.1905	0.0010	999.82	16.3	3 735	0.07047	0.167 ×10⁻²	1875	13.4×10⁻⁷	0.0365	19.5	0.232×10⁷
.4145			21.5	3 141	.07149	.161					
.3505			19.6								
.1829			14.7								
.1631			14.2	3 495	.07105						
.1097	.0005			6 512	.06930	.165					
.1798				3 735	.07047	.143					
.2713			18.8	3 955	.07047	.134					
.1798			14.2	4 381	.07003	.108					
Mach 8 tests — ambient-temperature-water injection										
0.1118	0.0005	999.82	22.0	3 467	0.07135	2.31 ×10⁻²	1210	38.3×10⁻⁷	0.0365	7.95	0.232×10⁷
.1753			30.1			4.23	1219				
.1295			30.4			4.04	1234				
.1576			29.9			3.98	1236				
.0734			24.0			3.97	1236				
.1608	.0002		29.4			2.23	1231				
.1024			23.5			2.23	1231				
.1015			30.4			4.08	1236				
.3121	.0005		39.8			2.30	1222				
.1573			30.1			2.24	1231				
.1012			24.0			2.23	1231				
.2644			40.3			3.92	1244				
.1362			29.4			3.93	1242				
.1271			24.0			.99	1213			7.80	
.2006			27.3			1.09	1134			7.80	
Mach 8 tests — heated-water injection										
0.0387	0.0002	999.82	37.7	15 202	0.06711	2.4119×10⁻²	1207	38.3×10⁻⁷	0.0365	7.95	0.232×10⁷
.0235			37.7	36 485	.06420	2.4119	1207				
.0164			38.1	52 476	.06274	4.04	1228				
.0247	.0005		39.0	36 149	.06463	2.43	1201				
.1820			38.1	64 877	.06186	3.98	1237				
.0229			37.1	38 328	.06390	1.05	1183			7.80	
.0306			52.4	32 415	.06449	2.43	1201			7.95	
.0321			52.6	42 039	.06361	4.01	1237				
.0158			25.7	36 772	.06405	2.22	1244				
.0429			52.5	36 676		2.22	1234				
.0365			51.8	36 772		3.97	1237				

ᵃThis test was run with nine orifices of the size shown, mounted in the vicinity of the stagnation point.

TABLE II.- RATIOS OF ORIFICE LENGTH TO DIAMETER

FOR TESTS AT $M = 6$ AND $M = 17.5$

d_O		l/d_O
ft	m	
M = 6		
0.0080	0.0024	3.0
.0026	.0008	9.1
M = 17.5		
0.0008	0.0002	1.5
.0013	.0004	.94
.0021	.0006	.59